# Low-Complexity Frequency Offset Estimation for Probabilistically Shaped MQAM Coherent Optical Systems

Wentao Liu, Tao Yang, Xue Chen, *Member, IEEE*, and Jialin You

***Abstract*—Since the reduction of the proportion of high modulus constellation points with $\pi/4 + k\pi/2$ ($k = 0, 1, 2, 3$) modulation phase in probabilistically shaped (PS)-*M*-ary quadrature amplitude modulation (MQAM) deteriorates the power spectrum peak of frequency offset from the 4th power signal, the conventional 4th power Fast Fourier Transform (FFT) algorithm is not suitable for PS-MQAM under moderate or strong shaping. In this paper a low-complexity multi-format frequency offset estimation (FOE) scheme is proposed, where the coarse estimation is based on extended quadrature phase shift keying (QPSK) partitioning and quasi-linear approximation in polar coordinates at the first stage, and the fine estimation in subsequent stage using Digital Amplification and 4th power FFT with Sparse Operation. The computational complexity is approximately reduced by 71% compared with radius directed (RD) 4th power FFT algorithm with the same mutual information (MI) performance under 2e-2 bit error rate (BER). Dual polarization (DP) PS-16/32/64QAM numerical simulations prove that the normalized mean square error (NMSE) of proposed FOE scheme is an order of magnitude lower than that of RD 4th power FFT algorithm. The higher FOE accuracy has been demonstrated experimentally in DP PS-16/32QAM systems.**

***Index Terms*—Frequency offset estimation, probabilistically shaped, coherent optical communication, M-quadrature amplitude modulation, low-complexity.**

## I. Introduction

PROBABILISTIC shaping (PS) has been widely considered as a promising digital transmission technique for flexible coherent optical communication systems [1]–[4]. PS constellation symbols are transmitted with different priori probabilities. Usually the larger modulus symbols are transmitted with lower probabilities. Compared with uniform *M*-ary quadrature amplitude modulation (MQAM) format, PS-MQAM not only achieves some shaping gain, but also offers fine-grained and flexible information rate to adapt different transmission link conditions [4]–[8].

For the uniform MQAM, some frequency offset estimation (FOE) algorithms have been proposed in recent years. The improved algorithms based on *Mth*-power are proposed in [9], [10], but those are not suitable for high-order QAM systems. The joint schemes for carrier frequency offset and phase recovery based on adaptive Kalman filter are proposed in [11], [12], but adaptive Kalman filter has initial value sensitivity and poor stability under low OSNR. For stable and high estimation accuracy, the method of FFT deployed for FO estimation after 4th power operation (4th power FFT) is the main choice [13]–[16]. However, for PS-MQAM, the reduction of the proportion of high modulus constellation points with $\pi/4 + k\pi/2$ ($k = 0, 1, 2, 3$) modulation phase (called QPSK-points that is main contributor for FOE) under moderate or strong shaping deteriorates the performance of the conventional 4th power FFT algorithm. To estimate accurately the frequency offset (FO) in PS-MQAM system, pilot-based FOE is employed in [18], but pilot insertion reduces spectrum efficiency (SE) by about 2%–5%. In [17], the generalized circular harmonic expansion (GCHE) algorithm is proposed, but accurate signal-to-noise ratio (SNR) of the signal needs to be known before FOE. The radius directed (RD) 4th power FFT algorithm based QPSK-selection is studied in [17], [19], [20]. The algorithm adds a decision operation to 4th power FFT with the long FFT size, which further increases the computational complexity of the FOE. Therefore, a blind, low-complexity, high-accuracy FOE algorithm for PS systems needs to be further studied.

In this paper, we propose a low-complexity blind FOE scheme in the flexible PS-MQAM system. Although the proportion of high modulus QPSK points decreases, the proportion of low modulus QPSK points and near the constellation points with $\pi/4 + k\pi/2$ ($k = 0, 1, 2, 3$) modulation phase that is referred to QPSK-like points do not decrease or even increase under moderate or strong shaping. Therefore, the coarse estimation is based on extended QPSK partitioning and quasi-linear approximation in polar coordinates at the first stage. The innermost QPSK points and the second inner QPSK points occupy a high proportion in the PS-MQAM under moderate or strong shaping, so the fine estimation in subsequent stage taking advantage of the above these points' features, amplifying these points digitally and performing 4th power FFT to guarantee the precision

Manuscript received 10 April 2022; revised 16 June 2022; accepted 6 July 2022. Date of publication 12 July 2022; date of current version 27 July 2022. This work was supported in part by the Beijing Municipal Natural Science Foundation under Grant 4214059, in part by the National Natural Science Foundation of China under Grant 62001045, in part by the State Key Laboratory of IPOC under Grant IPOC2021ZT17, and in part by the Fundamental Research Funds for the Central Universities under Grant 2022RC09. *(Corresponding authors: Tao Yang, Xue Chen.)*

The authors are with the State Key Laboratory of Information Photonics and Optical Communications, Beijing University of Posts and Telecommunications, Beijing 100876, China (e-mail: lwt1992@bupt.edu.cn; yangtao@bupt.edu.cn; xuechen@bupt.edu.cn; youjialin@bupt.edu.cn).

Digital Object Identifier 10.1109/JPHOT.2022.3189993

TABLE I
CONSTELLATION ENTROPIES OF PS-16/32/64QAM IN DIFFERENT LAMBDA

| PS-16QAM | | PS-32QAM | | PS-64QAM | |
|---|---|---|---|---|---|
| lambda | constellation entropies | lambda | constellation entropies | lambda | constellation entropies |
| 0 | 4 | 0 | 5 | 0 | 6 |
| 0.05 | 3.94 | 0.03 | 4.92 | 0.01 | 5.95 |
| 0.1 | 3.79 | 0.05 | 4.79 | 0.02 | 5.84 |
| 0.15 | 3.56 | 0.08 | 4.51 | 0.03 | 5.67 |
| 0.2 | 3.31 | 0.1 | 4.3 | 0.04 | 5.47 |
| 0.25 | 3.05 | 0.12 | 4.1 | 0.05 | 5.27 |
| 0.3 | 2.83 | 0.15 | 3.81 | 0.06 | 5.08 |
| 0.35 | 2.63 | 0.18 | 3.56 | 0.07 | 4.89 |
| 0.4 | 2.48 | 0.2 | 3.41 | 0.08 | 4.71 |
| 0.45 | 2.35 | 0.22 | 3.28 | 0.09 | 4.56 |
| 0.5 | 2.26 | 0.25 | 3.15 | 0.1 | 4.41 |

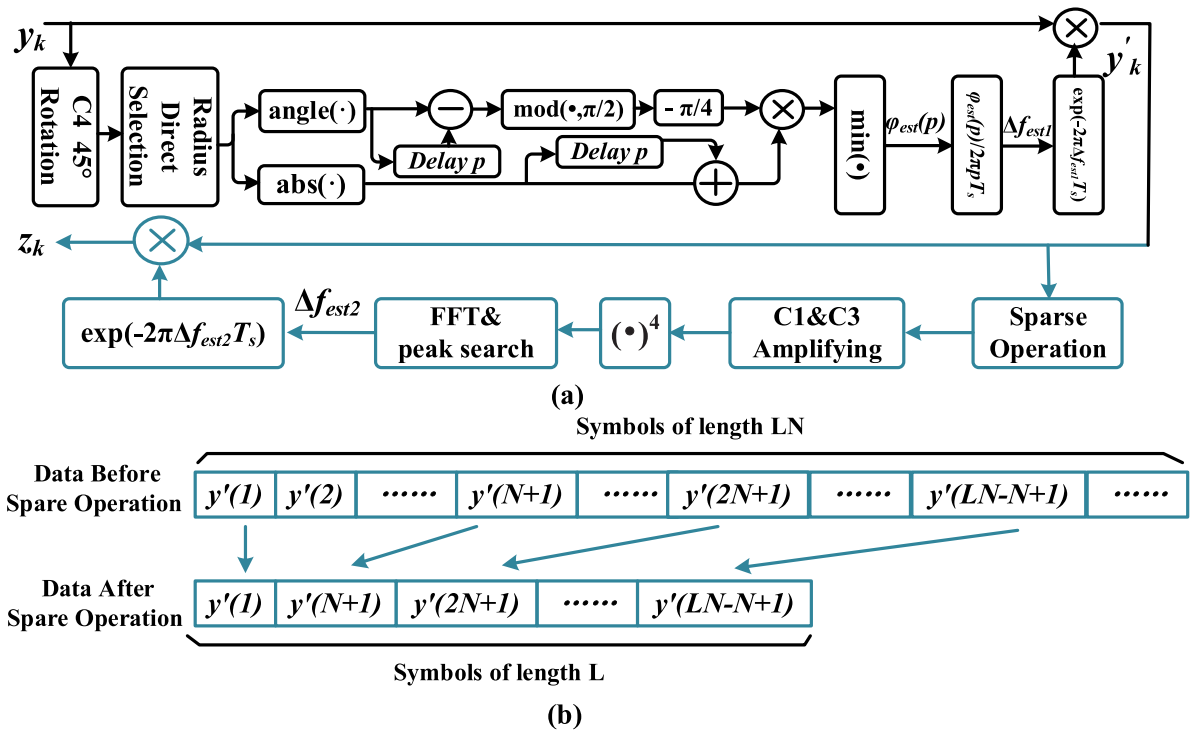


Fig. 1. (a) Block diagram of the proposed FOE algorithm. (b) Sparse Operation in the second stage FOE.

and further reduce the overall complexity by sparse operation. Section II introduces the PS technique briefly and the principle of the proposed two-stage FOE algorithm. Section III presents the simulation verification results. In Section IV, the computation complexity of proposed algorithm is analyzed. Section V shows the experimental results. Lastly, Section VI summarizes the paper.

## II. PROBLEM DESCRIPTION AND THE PROPOSED DSP SCHEME

PS based on a distribution matcher has been proposed to generate the PS-MQAM signal with flexible entropies [21]. In general, PS is implemented by applying the Maxwell Boltzmann (MB) distribution to the a-priori probabilities $P_X(x)$ of symbols $x$ [22]:

$$P_X(x) = \frac{e^{-\lambda|x|^2}}{\sum_{i=1}^{C} e^{-\lambda|x_i|^2}} \tag{1}$$

where λ is the shaping factor (SF) and $C$ is the modulation order of MQAM. The entropy of PS-MQAM signal is:

$$H(X) = -\sum_{i=1}^{C} P_X(x_i)\log_2(P_X(x_i)) \tag{2}$$

According to (1) (2), different λ corresponds to different entropy $H(X)$. Table I shows the constellation entropies of PS-16/32/64QAM in different λ. For intuitive understanding of PS, Fig. 3(a)–(c) show constellation probability distribution histograms of 0.06 PS-16QAM/32QAM/64QAM, respectively. Maximizing the channel capacity is the criterion for selecting constant λ that determines the probability distribution of constellation. For conciseness, we use the notation λ-PS- MQAM to denote the PS-MQAM constellation with λ. In this paper, we use the mutual information (MI) that is an upper bound on the achievable information rate as a performance indicator because

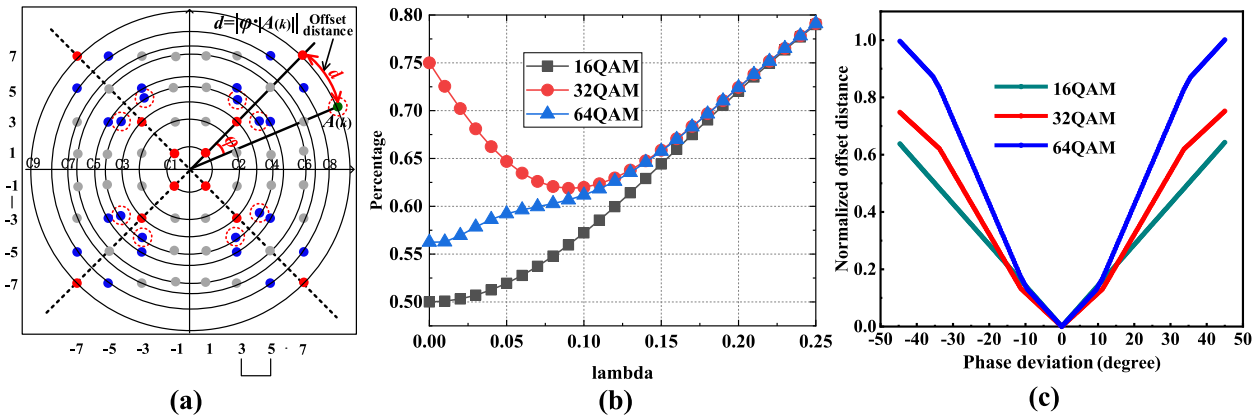


Fig. 2. (a) the principle of the extended constellation partitioning and offset distance calculation. (b) the percentage of constellation points used in the first-stage FOE under different SF. (c) Offset distance as a function of the phase deviation induced by FO.

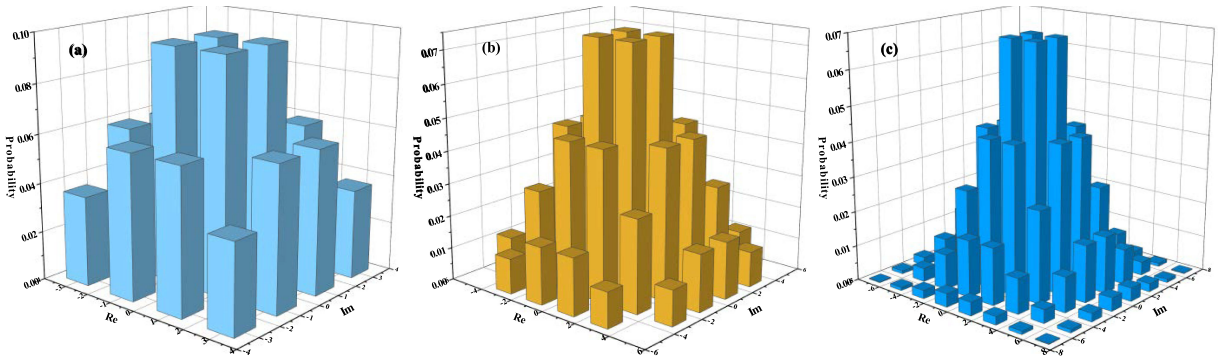


Fig. 3. Constellation probability distribution histograms of 0.06 (a) PS-16QAM (b) PS-32QAM (c) PS-64QAM.

we just investigate FOE algorithms but do not involve specific PS coding or decoding schemes [15], [23].

At the receiver, the digitalized samples after optical-to-electrical conversion and analog-to-digital (ADC) conversion with various impairments are sent to the DSP module for compensation. After IQ imbalance compensation, chromatic dispersion (CD) compensation, timing recovery, polarization de-multiplexing and the adaptive channel equalization, the recovered signal $y_k$ with the frequency offset (FO) and laser linewidth induced phase noise can be expressed as:

$$y_k = x_k e^{j(2\pi \Delta f k T_s + \theta_k)} + n_k \tag{3}$$

where $x_k$ is the transmitted symbol and $n_k$ is a Gaussian random variable with zero mean and variance ${\sigma_n}^2$. $\Delta f$ is the FO between transmitter and local oscillator (LO) lasers, and $\theta_k$ is the phase noise primarily introduced by the laser linewidth, which is modeled as a Wiener process. $T_s$ is the signal sampling period.

The first stage of FOE is based on extended QPSK partitioning and quasi-linear approximation. As shown in Fig. 1(a). In general, only QPSK points (highlighted by the red color) are utilized for FOE in the QPSK-Diff algorithm [24], which requires a long block size. To increase the proportion of available symbols within a shorter block length, QPSK-like points (highlighted by the blue color), including $\pi/4$ rotation C4, C5 and C8 symbols, can also be used for FOE [25]. Consequently, the number of available symbols increases from 8 to 24 for 32QAM and 12 to 36 for 64QAM.As shown in Fig. 2(a). The received symbols of QPSK points and QPSK-like points are selected for polar coordinate transformation and then the symbol modulus $A(k)$ and the phase data $\varphi(k)$ are stored. To take advantage of FO-related information in different timespan, multi-symbol differential phases are calculated as follows.

$$\Delta\varphi(k, k+p) = \varphi[kT_s] - \varphi[(k+p)T_s], p = 1, 2, 3, \ldots, P \tag{4}$$

where $p$ is the number of symbol intervals. Note that the maximum value of $p$ is $P$. The phase noise introduced by the laser linewidth between $P$ symbols is basically unchanged, so the phase noise $\theta_k$ can be almost removed in the phase difference of any two symbols with $p$ period intervals. Then three $\Delta\varphi_i(k,\ k+p)$ $(i = 1, 2, 3)$ are obtained by adding three test phases (0 and $\pm\pi/6$) to $\Delta\varphi$, respectively. After that, $\Delta\varphi_i(k,\ k+p)$ $(i = 1, 2, 3)$ contain the modulation phase difference of the symbols, the phase noise introduced by the FO, and the added test phase (0 and $\pm\pi/6$).

$$\begin{aligned} \Delta\varphi_1(k, k+p) &= \Delta\varphi - \pi/6 \\ \Delta\varphi_2(k, k+p) &= \Delta\varphi \\ \Delta\varphi_3(k, k+p) &= \Delta\varphi + \pi/6 \end{aligned} \tag{5}$$

Next, the modulo $\pi/2$ and the minus $\pi/4$ operations on the $\Delta\varphi_i(k, k+p)$ are performed to remove modulated data phases and reference phase, respectively.

$$\varphi_i(p) = \mathrm{mod}(\Delta\varphi_i(k, k+p), \pi/2) - \pi/4 \tag{6}$$

Then weighted offset distance $d$ is adopted to improve robustness of FOE as follows.

$$d_i(p) = \sum_{k=1}^{K} [|\varphi_i(p)| \cdot (|A(k)| + |A(k+p)|)] \tag{7}$$

where $K$ is the number of symbols required for differential phase operation. Fig. 2(c) illustrates the offset distance $d_i(p)$ as a function of phase deviation $\varphi_i(p)$ for MQAM signals. From the figure we can see that the optimal $\varphi_i(p)$ which minimizes the $d_i(p)$ can be determined by finding the intersection of these two quasi straight lines. Thanks to the symmetry of the two lines, we can easily calculate the intersection by only three points distributed on the two straight lines. Three points lying on symmetrical quasi-straight line can be obtained. Firstly, we get the two points with largest and smallest $d_i(p)$ by comparing, and we determine *Line* 1 through these two points by taking advantage of the symmetry and periodicity of the curve. Then, we use the inverse of the slope of *Line* 1 and another point information to determine *Line* 2. Finally, we calculate the intersection of *Line* 1 and *Line* 2, and the abscissa value of the intersection is the required value $\varphi_{est}(p)$. $\varphi_{est}(p)$ represents the optimal $\varphi_i(p)$. The phase angle $\varphi_{est}(p)$ which minimizes the offset distances $d_i$ can be directly determined by finding the intersection of these two quasi straight lines [26]. Lastly, $\Delta f_{est1}$ can be estimated by averaging all $P$ results as follows.

$$\Delta f_{est1} = \frac{1}{P} \sum_{p=1}^{P} \varphi_{est}(p)/2\pi p T_s \tag{8}$$

Because $-\pi/4 < \varphi_{est}(p) < \pi/4$, the FOE range based on each $\varphi_{est}(p)$ is $[-1/(8T_s), 1/(8T_s)]$, which shows the same estimation range as 4th power FFT.

As the SF increases, the available constellation points of 16/64QAM for the first-stage FOE increase and the proportion of 32QAM available constellation points is still higher than 60%, which is illustrated in Fig. 2(b). So, the first-stage FOE we proposed is suitable for PS system. However, with the increase of SF, constellation points having the high modulus with high noise immunity reduce rapidly, which leads to the deterioration of the stability and robustness of the algorithm. It cannot meet the requirement of the accuracy for FOE in the case of low signal-to-noise ratio (SNR). Therefore, a second-level FOE algorithm based on digital amplification and 4th power FFT is proposed for residual frequency offset estimation (RFOE).

To improve RFOE accuracy without remarkably increasing the computational complexity, one sample is taken at intervals of $N$ samples before C1&C3 amplifying and FFT, which is called sparse operation. Then the extracted samples are spliced together to construct a data block for RFOE. As shown in Fig. 1(b), the negative effect of sparse operation is that RFOE range is reduced to $1/N$ of the original one. Too large $N$ causes the second-stage RFOE range to be smaller than the residual FO after the first-stage FOE. Therefore, the value of $N$ should take into account the tradeoff between the scheme complexity/FOE accuracy and RFOE range. Too long symbols for FOE will result in the penalty from laser frequency drift. Next, we select C1&C3 rings and their amplitudes of those points are digitally amplified up to a relatively large value of 1.2 times of the MQAM maximum modulus. In order to optimize the parameters used in the proposed scheme, the threshold in the radius-directed process is investigated in simulation. For DP PS-32QAM/PS-64QAM, $0.45*(R_1 + R_2)$, $0.55*(R_2 + R_3)$ and $0.45*(R_3 + R_4)$ are chosen as the optimal thresholds, while they are $0.5*(R_1 + R_2)$ and $0.5*(R_2 + R_3)$ in DP PS-16QAM systems, here $R_1$, $R_2$, $R_3$ and $R_4$ are the modulus of C1, C2, C3 and C4 ring, respectively [17], [32]. Please note that the amplified modulus is enough for peak searching. If the amplified modulus is too large, the role of non-digitally-amplified constellation points is greatly weakened in the process of spectrum peak search and some constellation points near modulus C1&C3 are misjudged as the constellation points with modulus C1&C3 at low OSNR. The misjudged high modulus constellation points cannot remove the modulation phase completely, so the spectrum will become messy at low OSNR. The operation is illustrated in Fig. 4(b) and (c). Finally, the 4th power and the FFT& spectrum peak search are performed on data block of length $L$ as follows.

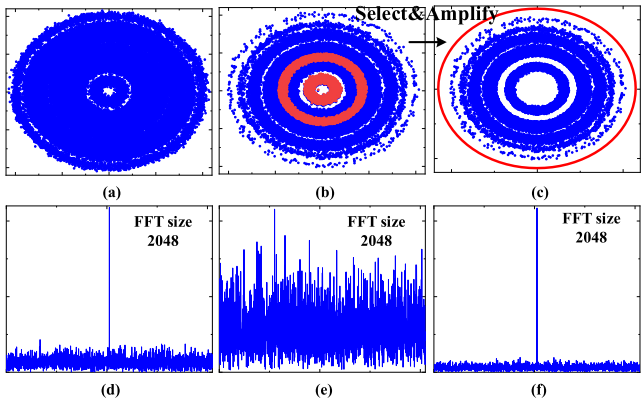


Fig. 4. Constellation diagrams before FOE and 4th power signal' spectrum, (a) uniform 64QAM (b) PS-64QAM (c) PS-64QAM with amplified C1&C3 rings (red ones in (b)), (d) the spectrum of 4th power signal (a), (e) the spectrum of 4th power signal (b), (f) the spectrum of 4th power signal (c).

$$y'^4(kNT_s) = A^4(kNT_s)\exp[j8\pi\Delta f_{res.}kNT_s + 4j\theta(kNT_s)] + n'(kNT_s) \tag{9}$$

$$\Delta f_{est2} = \frac{1}{4} \underset{f\in[-R_s/2N, R_s/2N]}{\arg\max} \left| \sum_{k=1}^{L} y'^4(kNT_s) e^{-j2\pi f kNT_s} \right| \tag{10}$$

where $A(\bullet)$ represents the modulus of the samples and $\Delta f_{res.}$ is the residual FO after the first-stage FOE. The estimation range for the second-stage method is $[-1/(8NT_s); 1/(8NT_s)]$, with a resolution of $1/(4LNT_s)$. It can be seen that the lager $N$ is to ensure higher accuracy of FOE.

TABLE II
OSNR CORRESPONGDING TO THE 2E-2 BER UNDER DIFFERENT LAMBDA IN DP PS-MQAM SYSTEM

| 128Gbaud DP PS-16QAM | | 108Gbaud DP PS-32QAM | | 96Gbaud DP PS-64QAM | |
|---|---|---|---|---|---|
| lambda | OSNR (dB) | lambda | OSNR (dB) | lambda | OSNR (dB) |
| 0 | 23.3 | 0 | 25.3 | 0 | 27.4 |
| 0.05 | 22.5 | 0.03 | 24.5 | 0.01 | 26.8 |
| 0.1 | 21.8 | 0.05 | 23.8 | 0.02 | 26.1 |
| 0.15 | 21 | 0.08 | 22.8 | 0.03 | 25.4 |
| 0.2 | 20.3 | 0.1 | 22.3 | 0.04 | 24.7 |
| 0.25 | 19.5 | 0.12 | 21.5 | 0.05 | 24 |
| | | 0.15 | 20.6 | 0.06 | 23.5 |
| | | 0.18 | 19.8 | 0.07 | 22.8 |
| | | 0.2 | 19.3 | 0.08 | 22.3 |
| | | | | 0.09 | 21.9 |
| | | | | 0.1 | 21.5 |

Consequently, the first-stage FOE algorithm gives stable coarse estimation results and ensures that the FOE range is $[-1/8T_s; 1/8T_s]$, which shows the same estimation range as 4th power FFT. Then the second-stage FOE algorithm guarantees resolution of FFT without increasing or even reducing the FFT size, thereby ensuring overall frequency offset estimation accuracy of the two-stage algorithm, which satisfies the requirement for FOE accuracy in PS system.

## III. NUMERICAL SIMULATIONS

To investigate the performance of our proposed two-stage FOE algorithm in 800Gbps data rate coherent systems, 128 GBaud DP PS-16QAM/108 GBaud DP PS-32QAM/96 GBaud DP PS-64QAM optical back-to-back (B2B) simulation platforms are constructed. Conventional 4th power FFT [27] and RD 4th power FFT without interpolation [11] algorithms are done for the purpose of comparison. In order to optimize the parameters used in RD 4th power FFT, the threshold in the radius-directed process is investigated in simulation. $0.45*(R_1 + R_2)$ is chosen as the optimal threshold for DP PS-32QAM/PS-64QAM, while it is $0.5*(R_1 + R_2)$ in DP PS-16QAM systems, here $R_1/R_2$ is the modulus of C1/C2 ring, respectively [17], [32]. Different values of FO are set and additive white Gaussian noise (AWGN) is loaded to obtain different OSNR. Before performing FOE, I/Q imbalance, timing error and polarization impairments are adequately compensated [28]. The phase noise from laser linewidth is not compensated before the FOE. The laser linewidth of the transmitter and the local oscillator (LO) is set to 100 kHz uniformly. The normalized mean square error (NMSE) performance with different SF of 4th power FFT /RD 4th power FFT and proposed FOE algorithms are shown in the first row of Fig. 6. Since the overall proposed FOE accuracy depends on the estimation accuracy of the second-stage, it is enough for $P$ in (4) to take a value of 2. Please note that the value of $N$ in (10) is set to 8 in the simulation. The NMSE is defined as [17], [25]:

$$NMSE = \sum_{i=1}^{1000} \frac{|\Delta f_{est,i} - \Delta f_i|^2}{R_S^2} \tag{11}$$

where $\Delta f_{est,i}$ and $\Delta f_i$ denote the estimated and actual FO in the $i$th trial. $R_S$ is the symbol rate. For each measurement of the NMSE, the results are obtained over 1000 simulations, and for each simulation the FO is randomly and uniformly chosen from $[-1/8T_s, 1/8T_s]$. Please note that the sampling rate of input signal for FOE is equal to the symbol rate. The FOE range is also presented as $[-R_s/8, R_s/8]$. NMSE is calculated under the OSNR corresponding to the 2e-2 bit error rate (BER). As shown in Table II, the OSNR corresponding to the 2e-2 BER is a function of lambda in DP PS-MQAM system. Since NMSE is closely related to the data block size $L$ of FOE, for conciseness we use the notation $L$ FOE algorithm to denote the FOE algorithm with data block size $L$. For example, 1024 4th power FFT denotes the 4th power FFT algorithm with data block size 1024. As shown in Fig.6(a)–(c), the results indicate that the proposed two-stage FOE algorithm and RD 4th power FFT algorithm of different data blocks perform well, whereas the NMSEs of Polar-Diff algorithm (the first stage of our proposed algorithm) hovers in the range of 1e-6∼1e-5, which does not meet the system requirements for the accuracy of FOE. However, the NMSE results can also show that the residual frequency offset of Polar-Diff algorithm is stable in the order of 100MHz. When the SF increases to or even bigger than 0.15/0.04, conventional 1024 4th power FFT cannot work in DP PS-16QAM/PS-64QAM system. Meanwhile, conventional 1024 4th power FFT is also not suitable for DP PS-16QAM system. Furthermore, it can be seen from the smooth straight line in the figure that as the SF increases, the NMSE of the RD 4th power FFT, Polar-Diff. and proposed FOE scheme basically does not change under fixed FOE block size. Fig. 5 shows the NMSE versus block size of RD 4th power FFT, Polar-Diff. and proposed FOE scheme. The block size of the first-stage FOE in Fig. 5(c) is randomly selected at [512, 1024, 2048]. As FOE block size increases, the NMSE decreases and the FOE accuracy increases. But Polar-Diff. (the first-stage of proposed FOE scheme) does not meet the requirements of the FOE accuracy of PS-MQAM system. So the second-stage of proposed FOE is required, whose NMSE stands for the NMSE of proposed FOE as a whole. Furthermore, compared to RD 4th power FFT, the two-stage scheme of our proposed adopts a smaller FFT size to obtain a lower NMSE. For example, the NMSE of the two-stage scheme with 512 FFT size is ∼6e-10, while the NMSE of RD 4th power FFT with 2048 FFT size is ∼2e-9 in 96 GBaud DP PS-64QAM system. The second row of Fig. 6 shows the NMSE with the actual FO in DP 0.1-PS-16QAM/0.06-PS-32QAM/0.03-PS-64QAM system respectively. For PS-16QAM/PS-64QAM, in order to

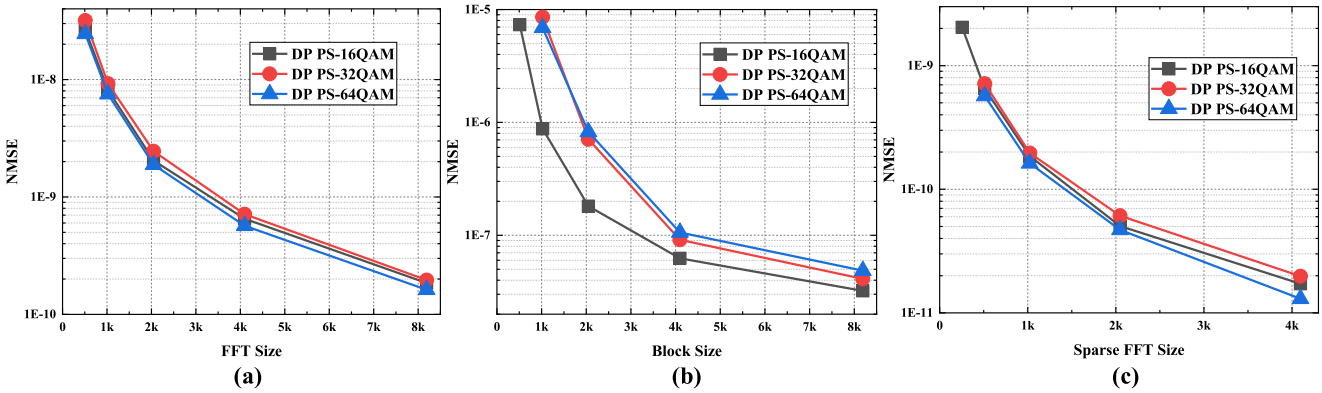


Fig. 5. The NMSE versus block size of (a) RD 4th power FFT (b) Polar Diff. (c) the proposed FOE in optical B2B DP PS-MQAM systems. NMSE is calculated under the OSNR corresponding to the 2e-2bit error rate (BER). The FO is randomly and uniformly chosen from $[-1/8T_s,\ 1/8T_s]$ for each realization. The sparse factor $N$ is 8.

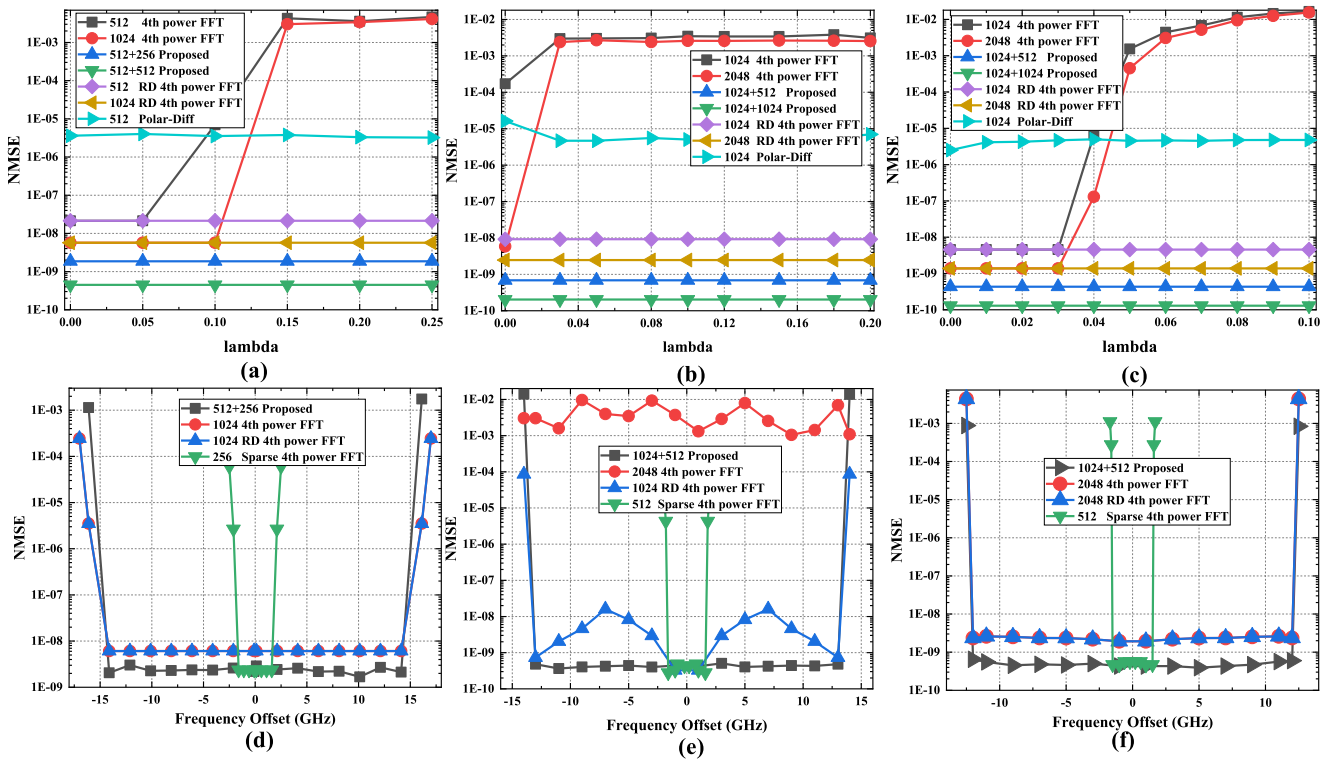


Fig. 6. The NMSE versus SF (first row)/FO (second row) in optical B2B (a) DP PS-16QAM (b)DP PS-32QAM (c) DP PS-64QAM (d) DP 0.1-PS-16QAM (e) DP 0.06-PS-32QAM (f) DP 0.03-PS-64QAM systems. NMSE is calculated under the OSNR corresponding to the 2e-2 bit error rate (BER). The FO is randomly and uniformly chosen from $[-1/8T_s,\ 1/8T_s]$ for each realization.

facilitate the NMSE performance comparison with conventional 4th power FFT, the SF is chosen as 0.1/0.03, respectively, although which does not belong to strong shaping. The FOE range of the proposed scheme is also presented as $[-R_s/8,\ R_s/8]$ under the three Modulation Formats (MFs), which is the same as that of the two comparison algorithms. The results indicate once again that for three MFs the proposed two-stage algorithm achieves more robust FOE with remarkably improved accuracy than that of conventional 4th power FFT and RD 4th power FFT algorithms. In addition, the estimation range of the second stage of the proposed scheme is shown as $[-R_s/64,\ R_s/64]$, which is far less than RD 4th power FFT algorithm. For example, in 96 GBaud DP PS-64QAM system the estimation range of that is only $[-1.5,\ 1.5]$ GHz which cannot satisfy the requirement for FOE range. Therefore, the result proves that the first-stage FOE is necessary to ensure stable coarse estimation results in PS system. The NMSE of FOE versus OSNR for three MFs, with the FO randomly chosen from $[-R_s/8,\ R_s/8]$, are shown in Fig. 7(a), (b) and (c), respectively. The OSNR of the proposed scheme are 20.8, 22.7 and 23.2 dB for 16, 32 and 64QAM, respectively, and 0.8, 1.9 and 1.5 dB higher than RD 4th power FFT algorithm under NMSE of 1e-8. Compared with our

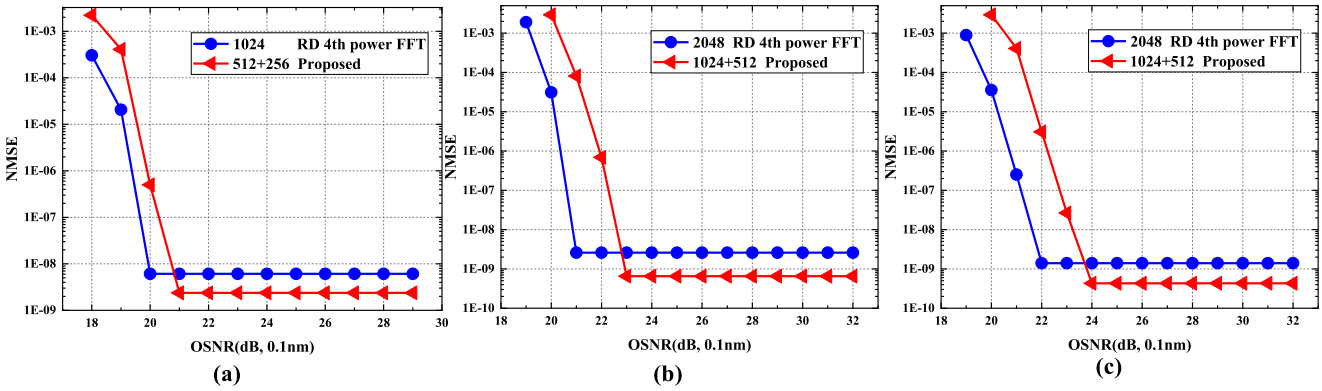


Fig. 7. The NMSE versus OSNR in the optical B2B (a) PM-PS-16QAM (b) PM-PS-32QAM (c) PM-PS-64QAM systems.

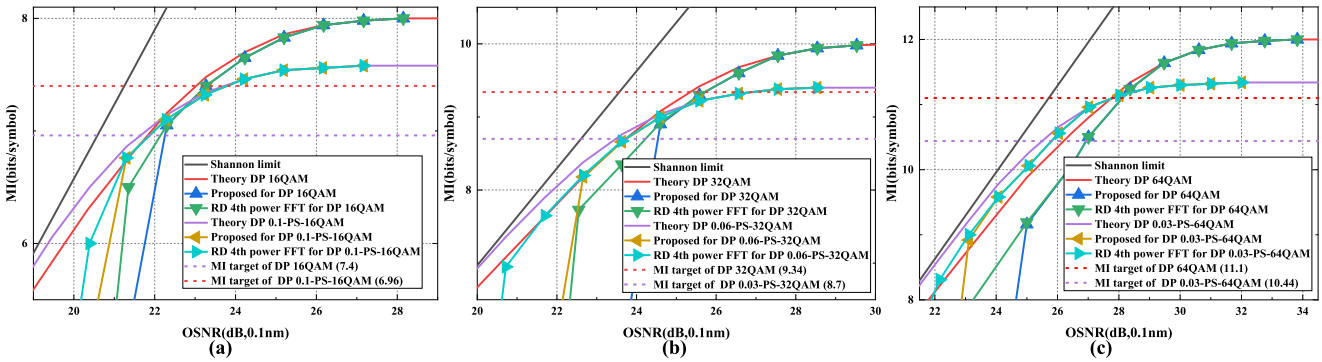


Fig. 8. The MI versus OSNR under B2B (a) DP PS-16QAM (b) DP PS-32QAM (c) DP PS-64QAM.

proposed FOE scheme, RD 4th power FFT has greater NMSE at low OSNR due to the inclusion of less unwanted constellation points without $\pi/4 + k\pi/2$ (k = 0, 1, 2, 3) modulation phase and a longer FFT size, which brings high computational complexity. Although the OSNR performance of our proposed FOE scheme is not as good as RD 4th power FFT algorithm's one, it has met the requirements of FEC soft-decision (SD) threshold of BER 2e-2 and the complexity of the proposed scheme is only about one third of the latter (see Section IV).

The MI performance versus OSNR for the six MFs is shown in Fig. 8. The curves of Shannon limit and the ideal MI is given as a benchmark. In the case of the same OSNR, the system MI calculation result using proposed scheme is the same as that of using RD 4th power FFT algorithm in PM-PS QAM system. Any practical architecture to combine it with FEC is not used in the simulation. The MI value under the soft-decision FEC threshold 2E-2 BER is used as the target MI. The theoretic FEC code rates for target MIs are 0.925/0.934/0.925 in the DP PS-16/32/64QAM system, respectively. The proposed two-stage scheme shows OSNR penalty of ∼0.2 dB with respect to the ideal one. The OSNR penalty is due to the imperfections of the simulation system, such as the bandwidth limitation of the low-pass filter and the limited number of bits of the DAC and ADC.

## IV. Computation Complexity Analysis

We compare the computational complexity in terms of the number of the operations (real multiplication, real addition, and comparison) among 4th power FFT, RD 4th power FFT and our proposed FOE scheme. When SF tuning range is [0,0.2], no more than 75% symbols in a block are used for the first stage FOE. Therefore, the computation complexity of the first-level of proposed scheme is calculated in the case of 75% symbols in a block available for FOE. The CORDIC in the first-stage FOE can be executed without multiplication, so we do not take the computational complexity of the CORDIC into account. All computational complexities are calculated for a single polarization. For the first-stage FOE, we have: 1) The extended QPSK partitioning operation takes $2N_1$ real multipliers, $N_1$ real adders and $2N_1$ comparators, while the rotation of C4 requires $N_1/4$ real adders and $3N_1/2$ comparators. 2) The rotation of the two angles ($-\pi/6$ and $\pi/6$) requires $3N_1/2$ real adders. 3) The calculation of the $\varphi_i$ requires $3N_1/2$ real adders and $3N_1/4$ comparators. 4) The calculation of the $d_i$ requires $2N_1$ real multipliers and $N_1$ real adders. 5) The calculation of the $\varphi_{est}$ requires 2 real multipliers, 3 real adders, and 3 comparators. In addition, the unwrapping operation requires 1 comparator and 1 real adder. Finally, the process of the frequency offset compensation requires 4 real multipliers, 2 real adders.

TABLE III
COMPLEXITY COMPARISON OF THREE METHODS ($N = 2048$, $N_1 = 1024$, $N_2 = 512$)

| Algorithm | Real multiplication | Real addition | Comparison |
|---|---|---|---|
| 4th power FFT | $2Nlog_2N+10N+2$ (65538) | $3Nlog_2N+5N$ (77824) | $N$ (2048) |
| RD 4th power FFT | $2Nlog_2N+12N+2$ (69634) | $3Nlog_2N+6N$ (79872) | $2N$ (4096) |
| Proposed | $4N_1+2N_2log_2N_2+27/2*N_2+8$ (20234) | $21/4*N_1+3N_2log_2N_2+6N_2+6$ (25350) | $17/4*N_1+4N_2+4$ (8452) |

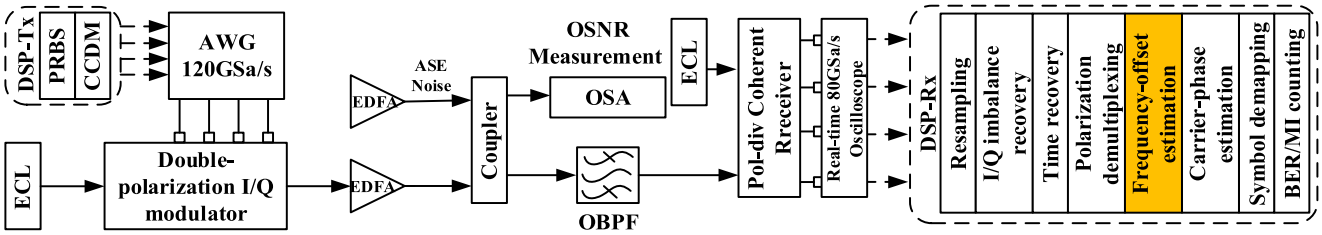


Fig. 9. Experimental setup for 40 GBaud DP PS-16QAM and 32 GBaud DP PS-32QAM systems.

For the second-stage FOE, we have: 1) The extended QPSK partitioning operation takes $2N_2$ real multipliers, $N_2$ real adders and $3N_2$ comparators. 2) The calculation of C1&C3 amplifying requires $3N_2/2$ real multipliers. 3) For the 4th power FFT, it takes $2N_2log_2N_2 + 10N_2 + 2$ real multipliers, $3N_2log_2N_2 + 5N_2$ real adders and $N_2$ comparators.

In conclusion, the overall computational complexity is summarized as shown in Table III. Taking PM-PS-64QAM as an example. $N$ generally takes the value of 2048. $N_1$ is 1024, and $N_2$ is 512. It can be observed that the multiplication computational complexity for proposed scheme is approximately reduced by 71% compared with RD 4th-FFT algorithm.

## V. EXPERIMENT AND RESULTS

To further investigate the performance of the proposed FOE scheme, 40 GBaud DP PS-16QAM and 32 GBaud DP PS-32QAM B2B experiments were carried out. Fig. 9 shows the experimental setup. At the transmitter, an integrated tunable external cavity laser (ECL) at 193.415 THz with ~50 kHz measured linewidth is used as a carrier laser. 4/6-level Gray mapped signals (Ix, Qx, Iy, Qy) are generated following uniform or MB distribution via Constant Composition Distribution Matching (CCDM) method [31]. Then, the signals are sent into 4 synchronized channels of arbitrary waveform generator (AWG, Agilent 8194A) working at 120 (96)-GSa/s with ~36 GHz 3 dB analog bandwidth. Threefold oversampling is performed to provide 40 (32) GBaud signals, which drive a polarization multiplexed optical I/Q modulator. The OSNR is controlled by the amplified spontaneous emission (ASE) noise produced in an erbium-doped fiber amplifier (EDFA). The ASE noise loaded into the system is coupled to the transmitted signal. OSNR is measured by an optical spectrum analyzer (OSA) under 0.1 nm noise reference bandwidth. Then, the signal is filtered using an optical band-pass filter (OBPF) with 0.8 nm bandwidth. At the receiver side, another ECL with ~50 kHz linewidth is used as the LO to realize coherent detection. The central wavelength of the LO can be adjusted at the receiver side to deliberately set the FO. The optical signal is sampled by an 80 GSa/s realtime sampling oscilloscope for offline processing. The offline DSP flow is also shown in Fig. 9. Firstly, samples are processed with resampling to 2 samples per symbol and orthogonalization for IQ imbalance compensation [29]. Then, after timing recovery [30], radius-directed equalization (RDE) algorithm are employed for the purpose of polarization division de-multiplexing. The FO is estimated by the three algorithms for 16/32QAM. The two-stage quasi-linear approximation (QLA) method [26] is subsequently carried out for carrier phase estimation and the block size of 80 and 26 are used for the two stages, respectively. Finally, more than $10^6$ symbols are used for BER/MI counting.

Fig. 10(a) and (b) show the NMSE versus OSNR performance for 40 GBaud DP 0.1-PS-16QAM and 32 GBaud DP 0.06-PS-32QAM in B2B system, respectively. The FOs estimated in the experiment are set about 0, 1 and 2 GHz. The calculation of NMSE is the result of statistical average under that three different FOs, and so is MI described later in the paper. Compared with 4th power FFT and RD 4th power FFT, the proposed scheme always offers significantly improved estimation accuracy (the normalized MSE is reduced by one order) in the OSNR region with BER below 2e-2. 4th power FFT fails to realize correct FOE within FFT size of 2048 samples because of no high modulus constellation points with $\pi/4 + k\pi/2$ ($k = 0, 1, 2, 3$) modulation phase for 32QAM. For DP PS-16QAM and DP PS-32QAM, Fig. 10(c) and (d) shows the system MI under proposed scheme and RD 4th power FFT algorithm. The system MI for both algorithms are the same under the condition of the same OSNR. The curves of Shannon limit and the ideal MI is given as a benchmark. We investigate that, at the target MI, the experiment results show an OSNR penalty of ~1.2 dB (2 dB) and ~2 dB (3 dB) with respect to the ideal one in 40 GBaud DP PS-16QAM (DP 16QAM) and 32 GBaud DP PS-32QAM (DP 32QAM) system, respectively. The bandwidth of electrical devices and

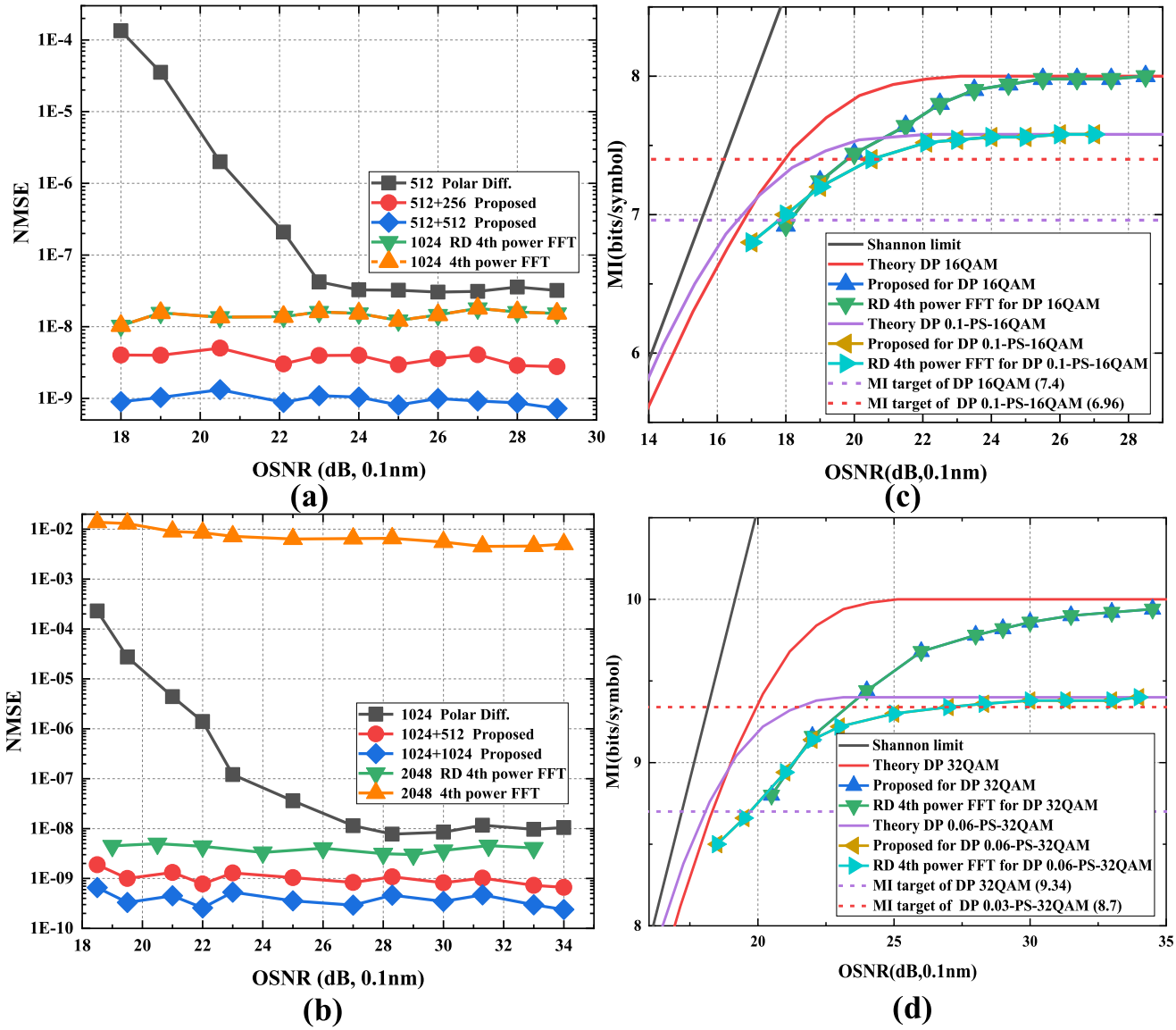


Fig. 10. (a) NMSE (c) MI versus OSNR for 40 GBaud DP PS-16QAM, (b) NMSE (d) MI versus OSNR for 32 GBaud DP PS-32QAM.

the nonlinear effect of IQ modulator are the main reasons for the penalty.

## VI. Conclusion

In this paper, we have proposed and demonstrated a low-complexity, blind FOE scheme for flexible PS-MQAM coherent optical systems. Taking advantage of the large proportion of QPSK points and QPSK-like points in the PS constellations, the coarse but robust first stage estimation based on extended QPSK partitioning and quasi-linear approximation in polar coordinates is implemented. The subsequent stage RFOE uses Sparse Operation combined with Digital Amplification to ensure high estimation accuracy. The computational complexity for proposed scheme is approximately reduced by 71% compared with RD 4th power FFT algorithm with the comparable FOE performance. For DP PS-16/32/64QAM, simulation results have demonstrated that the FOE's NMSE is reduced by an order of magnitude with FFT size being one fourth of RD 4th power FFT's. Meanwhile, 40 GBaud DP PS-16QAM and 32 GBaud DP PS-32QAM experiment results have further demonstrated that the proposed FOE algorithm can operate reliably with the block size being 1024(first stage) plus 512(second stage), when OSNR is above 19 dB.

## Appendix

1) The calculation of the $\varphi_{est}$ from $d_i$.
Three points lying on symmetrical quasi-straight line can be obtained and named $(-\pi/6, d_1)$, $(0, d_2)$ and $(\pi/6, d_3)$. Since these three points have six possible distributions in the linear interval, as shown in Fig. 11. Firstly, we get the two points with largest and smallest d by comparing, and we determine *Line* 1 through these two points by taking advantage of the symmetry and periodicity of the curve, as the solid line in the figure. Then, we use the inverse

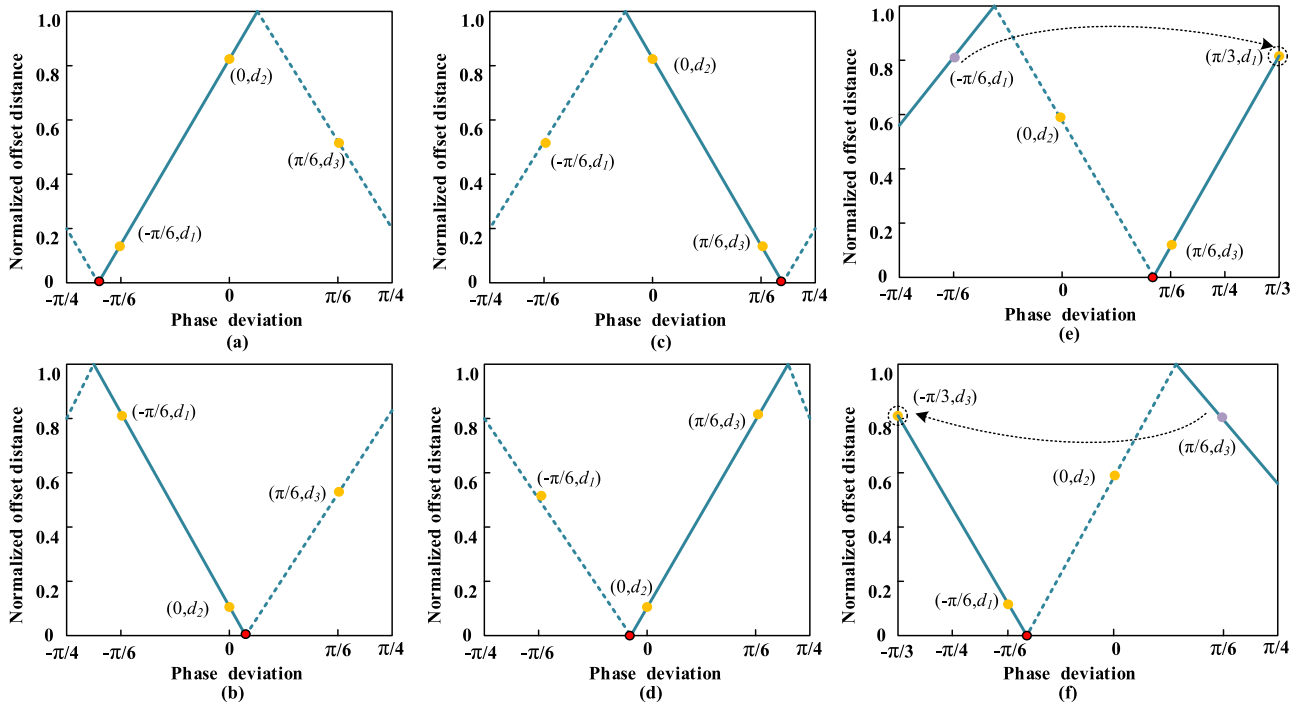


Fig. 11. Six possible distributions of normalized offset distance versus phase deviation.

of the slope of *Line* 1 and another point information to determine *Line* 2, as the dotted line in the figure. Finally, we calculate the intersection of *Line* 1 and *Line* 2, and the abscissa value of the intersection is the required value $\varphi_{est}$, as the red dot in the figure. In six different cases, the result of $\varphi_{est}$ is expressed as follows.

$$\varphi_{est} = \begin{cases} \frac{\pi(d_3-d_2)}{12(d_2-d_1)} - \frac{\pi}{6}, & d_2 > d_3, d_3 > d_1 \\ \frac{\pi(d_1-d_3)}{12(d_1-d_2)}, & d_1 > d_3, d_3 > d_2 \\ \frac{\pi(d_2-d_1)}{12(d_2-d_3)} + \frac{\pi}{6}, & d_2 > d_1, d_1 > d_3 \\ \frac{\pi(d_1-d_3)}{12(d_3-d_2)}, & d_3 > d_1, d_1 > d_2 \\ \frac{\pi(d_2-d_1)}{12(d_1-d_3)} + \frac{\pi}{6}, & d_1 > d_2, d_2 > d_3 \\ \frac{\pi(d_3-d_2)}{12(d_3-d_1)} - \frac{\pi}{6}, & d_3 > d_2, d_2 > d_1 \end{cases}$$

2) QPSK-like points.
The constellation points near $\pi/4 + k * \pi/2$ ($k = 0, 1, 2, 3$) and the constellation points near $\pi/4 + k * \pi/2$ ($k = 0, 1, 2, 3$) after $\pi/4$ rotation are defined as "QPSK-like points". As shown in Fig. 2(a). The symbols highlighted by blue points lying on C5 and C8 have phase offsets of only $\pm 14°$ and $\pm 9.5°$ from the diagonal lines with slope equal to $+1$ or $-1$, respectively. The symbols of C4 are rotated by $\pi/4$ so that the phase offsets of those symbols could be minimized to $\pm 11.3°$.

The degree for judging the phase offset is not fixed. The criterion is to let more constellation points participate in the first-stage FOE at the expense of no or few FOE performance, so as to reduce FOE block size and complexity.

## REFERENCES


[1] J. Cho and P. J. Winzer, "Probabilistic constellation shaping for optical fiber communications," *J. Lightw. Technol.*, vol. 37, no. 6, pp. 1590–1607, 2019.

[2] D. Pilori, L. Bertignono, A. Nespola, F. Forghieri, and G. Bosco, "Comparison of probabilistically shaped 64QAM with lower cardinality uniform constellations in long-haul optical systems," *J. Lightw. Technol.*, vol. 36, no. 2, pp. 501–509, 2018.

[3] J. Ren *et al.*, "A probabilistically shaped CAP modulation method employing multiple subsets mapping with symbol classification for a short reach communication," *IEEE Photon. J.*, vol. 11, no. 2, Apr. 2019, Art. no. 7901708.

[4] F. Buchali, F. Steiner, G. Böcherer, L. Schmalen, P. Schulte, and W. Idler, "Rate adaptation and reach increase by probabilistically shaped 64-QAM: An experimental demonstration," *J. Lightw. Technol.*, vol. 34, no. 7, pp. 1599–1609, 2016.

[5] J. Renner *et al.*, "Experimental comparison of probabilistic shaping methods for unrepeated fiber transmission," *J. Lightw. Technol.*, vol. 35, no. 22, pp. 4871–4879, 2017.

[6] T. Fehenberger, G. Böcherer, A. Alvarado, and N. Hanik, "LDPC coded modulation with probabilistic shaping for optical fiber systems," in *Proc. Opt. Fiber Commun. Conf.*, USA, 2015, pp. 1–3.

[7] L. Beygi, E. Agrell, J. M. Kahn, and M. Karlsson, "Rate-adaptive coded modulation for fiber-optic communications," *J. Lightw. Technol.*, vol. 32, no. 2, pp. 333–343, 2014.

[8] M. P. Yankov, D. Zibar, K. J. Larsen, L. P. B. Christensen, and S. Forchhammer, "Constellation shaping for fiber-optic channels with QAM and high spectral efficiency," *IEEE Photon. Technol. Lett.*, vol. 26, no. 23, pp. 2407–2410, Dec. 2014.

[9] J. Han, W. Li, Z. Yuan, Y. Zheng, and Q. Hu, "A simplified implementation method of Mth-power for frequency offset estimation," *IEEE Photon. Technol. Lett.*, vol. 28, no. 12, pp. 1317–1320, Jun. 2016.

[10] R. M. Ferreira *et al.*, "Optimized carrier frequency and phase recovery based on blind Mth power schemes," *IEEE Photon. Technol. Lett.*, vol. 28, no. 21, pp. 2439–2442, Nov. 2016.

[11] Q. Xiang, Y. Yang, Q. Zhang, and Y. Yao, "Modulation-transparent and Robust frequency offset and phase tracking scheme using self-learning Kalman filter for intelligent receiver," *J. Lightw. Technol.*, vol. 39, no. 23, pp. 7427–7434, 2021.

[12] X. Qian, Y. Yang, Q. Zhang, J. Cao, and Y. Yao, "Adaptive and joint frequency offset and carrier phase estimation based on Kalman filter for 16QAM signals," *Opt. Commun.*, vol. 430, pp. 336–341, 2019.
[13] B. Tang *et al.*, "Low complexity two-stage FOE using modified zoom-FFT for coherent optical M-QAM systems," *IEEE Photon. Technol. Lett.*, vol. 32, no.no. 5, pp. 263–266, Mar. 2020.
[14] J. Xiao *et al.*, "Low complexity FFT-based frequency offset estimation for M-QAM coherent optical systems," *IEEE Photon. Technol. Lett.*, vol. 27, no. 13, pp. 1371–1374, Jul. 2015.
[15] F. A. Barbosa, S. M. Rossi, and D. Mello, "Phase and frequency recovery algorithms for probabilistically shaped transmission," *J. Lightw. Technol.*, vol. 38, no. 7, pp. 1827–1835, 2020.
[16] D. A. A. Mello, F. A. Barbosa, and J. D. Reis, "Interplay of probabilistic shaping and the blind phase search algorithm," *J. Lightw. Technol.*, vol. 36, no. 22, pp. 5096–5105, 2018.
[17] Q. Yan, L. Liu, and X. Hong, "Blind carrier frequency offset estimation in coherent optical communication systems with probabilistically shaped M-QAM," *J. Lightw. Technol.*, vol. 37, no. 23, pp. 5856–5866, 2019.
[18] M. P. Yankov, E. P. da Silva, F. Da Ros, and D. Zibar, "Experimental analysis of pilot-based equalization for probabilistically shaped WDM systems with 256QAM/1024QAM," in *Proc. Opt. Fiber Commun. Conf.*, USA, 2017, pp. 1–3.
[19] S. Yao *et al.*, "Experimental analysis of fourier transform based blind frequency offset estimation for PS-QAM in W-band fiber-millimeter wave integrated system," in *Proc. Opt. Fiber Commun. Conf.*, USA, 2021, pp. 1–3.
[20] F. Xiao *et al.*, "Feed-forward frequency offset estimation for 32-QAM optical coherent detection," *Opt. Exp.*, vol. 25, no. 8, pp. 8828–8839, 2017.
[21] D. Pilori, "Advanced digital signal processing techniques for high-speed optical communications links," Ph.D. dissertation: Dept. Elect. Telecommun., Politecnico di Torino Univ., Torino, Italy, 2019.
[22] F. R. Kschischang and S. Pasupathy, "Optimal nonuniform signaling for Gaussian channels," *IEEE Trans. Inf. Theory*, vol. 39, no. 3, pp. 913–929, May 1993.
[23] A. Alvarado, E. Agrell, D. Lavery, R. Maher, and P. Bayvel, "Replacing thesoft-decision FEC limit paradigm in the design of optical communication systems," *J. Lightw. Technol.*, vol. 33, no. 20, pp. 4338–4352, 2015.
[24] I. Fatadin and S. J. Savory, "Compensation of frequency offset for 16-QAM optical coherent systems using QPSK partitioning," *IEEE Photon. Technol. Lett.*, vol. 23, no. 17, pp. 1246–1248, Sep. 2011.
[25] T. Yang *et al.*, "Hardware-efficient multi-format frequency offset estimation for M-QAM coherent optical receivers," *IEEE Photon. Technol. Lett.*, vol. 30, no. 18, pp. 1605–1608, Sep. 2018.
[26] T. Yang *et al.*, "Linewidth-tolerant and multi-format carrier phase estimation schemes for coherent optical M-QAM flexible transmission systems," *Opt. Exp.*, vol. 26, no. 8, pp. 10599–10615, 2018.
[27] M. Selmi, Y. Jaouen, and P. Ciblat, "Accurate digital frequency offset estimator for coherent PolMux QAM transmission systems," in *Proc. Eur. Conf. Opt. Commun.*, Austria, 2009, pp. 1–2.
[28] S. Savory, "Digital coherent optical receivers: Algorithms and subsystems," *IEEE J. Sel. Topics Quantum Electron.*, vol. 16, no. 5, pp. 1164–1179, Sep./Oct. 2010.
[29] I. Fatadin, S. J. Savory, and D. Ives, "Compensation of quadrature imbalance in an optical QPSK coherent receiver," *IEEE Photon. Technol. Lett.*, vol. 20, no. 20, pp. 1733–1735, Oct. 2008.
[30] M. Oerder and H. Mery, "Digital filter and square timing recovery," *IEEE Trans. Commun.*, vol. 36, no. 5, pp. 605–612, May 1988.
[31] P. Schulte and G. Bocherer, "Constant composition distribution matching," *IEEE Trans. Inf. Theory*, vol. 62, no. 1, pp. 430–434, Jan. 2016.
[32] D. Lavery, M. Paskov, and R. Maher, "Modified radius directed equaliser for high order QAM," in *Proc. Eur. Conf. Opt. Commun.*, Spain, 2015, pp. 1–3.